No.19 Journal of Petroleum Research & Studies (JPR&S)

Effect of CO_2 phase on its water displacements in a sandstone core sample: experimental study

تأثير طور غاز ثاني اوكسيد الكاربون على إزاحته للماء من نموذج رملي: دراسة مخبرية

Ebraheam Al-Zaidi*, Xianfeng Fan**

*Institute for Materials and Processes, School of Engineering, The University of Edinburgh, King's Buildings, Mayfield Road, Edinburgh, EH9 3JL, United Kingdom

**Corresponding author. Tel.: +44 0 131 6505678; fax: +44 0131 6506551.

E-mail address: x.fan@ed.ac.uk (X. Fan).

Abstract

CO_2 capture and storage have been considered as a key strategy to tackle CO_2 high concentrations in the atmosphere. The captured CO_2 is injected into deep saline aquifers, depleted hydrocarbon reservoirs and coal beds as gas, liquid, and/or supercritical phase. The CO_2 phase may affect its injection, migration, and displacement efficiency. Research work on CO_2 storage has mainly focused on the trapping mechanism, risk assessment, storage site selection, etc. However, CO_2 phase effect on its injection and displacement efficiency has largely been neglected. In this paper, experimental work was designed to investigate the impact of CO_2 phase on the pressure and production profiles as the experimental pressure increases.

The results show that CO_2 phase significantly affects the differential pressure profile, relative permeability of CO_2, and residual water saturation in a sandstone core sample. The differential pressure profiles of gaseous CO_2 and supercritical CO_2 phases were significantly different from that of liquid CO_2 phase, particularly before the CO_2 breakthrough. The increase in the experimental pressure caused an increase in the differential pressure profile of the sub critical CO_2 phases (gaseous and liquid CO_2) but a reduction in that of the supercritical phase. The relative permeabilities of the three CO_2 phases were in the range of 11-21 % while the residual water saturations (S_{wr}) were in the range of 36 to 42 %. In general, the relative permeabilities of both gaseous and supercritical CO_2 phases are quite close. The relative permeabilities of liquid CO_2 phase are higher. The increase in pressure caused an increase in the relative permeability and a decline in the S_{wr}. The scale of the change depends on CO_2 phase. Thus, our results reveal the high impact of CO_2 phase on its injection, and displacements efficiency.

1 Introduction

CO_2 capture and storage (CCS) is considered to be one of the promising techniques to reduce CO_2 emissions to the atmosphere. The captured CO_2 is stored into deep saline aquifers, depleted oil and gas reservoirs [1], or unminable coal beds [2, 3]. The injected CO_2 can also be utilized as a working fluid to enhance hydrocarbon recovery from oil and gas reservoirs, to enhance methane production from coal beds, or to extract geothermal heat from subsurface formations [2, 4]. In these subsurface formations, the injected CO_2 can exist in gas, liquid or supercritical phase as shown in Fig. (1) [5-7].

CO_2 phase has a significant impact on its wettability, and the interactions between CO_2, reservoir rock and the fluids in reservoir pore space. For example, the supercritical CO_2 has an ability higher than gas and liquid CO_2 to alter reservoir rocks towards less water-wetting state [8, 9]. An abrupt change in CO_2 phase can result in a significant change in its viscosity and density [3, 10]. Therefore, the change in CO_2 phase might have a significant impact on the differential pressure, entrance pressure, CO_2 injection rate, CO_2 displacement rate, CO_2 migration, and finally the stability of sored CO_2 and the efficiency of enhanced oil and gas recovery [5, 11].

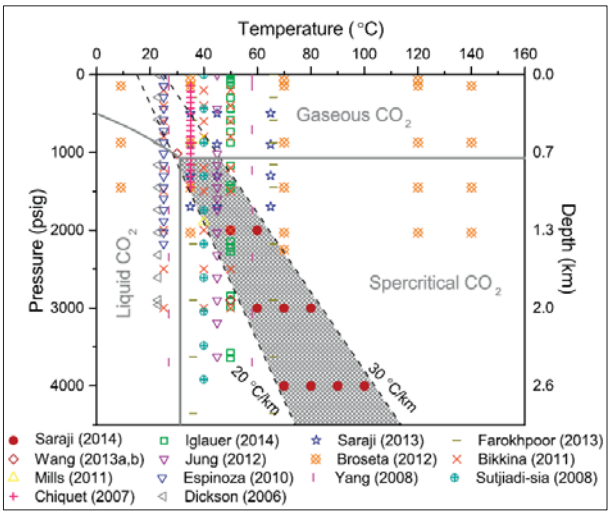

Fig. (1) The pressure and temperature ranges at which saline aquifers are found underground [12].

Extensive experimental and numerical research work has been designed to investigate CO_2 wetting and interfacial tensions under different pressure and temperature, relative permeability, capillary pressure-saturation, the impact of porosity heterogeneity on CO_2 migration and injection, CO_2 level and distribution, the sealing efficiency of caprocks, the effect of viscous stability on CO_2-brine flood front during immiscible displacements, and the optimization of CO_2 injection to maximize both CO_2 storage and enhance oil recovery (EOR), etc. The investigations have been conducted in a wide range of sandstone and carbonate core samples, such as: feldspar-rich sandstone, Berea sandstone, Nugget

sandstones, Tako sandstone, Bentheimer sandstone, Rothbach sandstone [4, 5, 7, 13-25]; [26, 27].

However, the extensive research has been focused on various aspects of supercritical CO_2. For example, Herring et al. investigated the capillary pressure-saturation for supercritical CO_2 ($scCO_2$) and brine at 37.5 ^{0}C and 83 bars [13]. Saeedi et al. [25] investigated $scCO_2$-brine displacements in different sandstone samples with the emphasis on the effect of cyclic CO_2-brine on differential pressure and saturation profiles. Chang et al. [28] conducted both drainage and imbibition CO_2-core flooding of supercritical CO_2 and water on low permeability sandstone core samples under a pressure higher than 80 bars and at a temperature of 40 ^{o}C to study the dynamic drainage process of water by supercritical CO_2.

To the authors' best knowledge, there is no such investigations into the effect of CO_2 pressure on the differential pressure profile and production performance as a function of CO_2 phase. In this paper, laboratory dynamic CO_2-water drainage experiments were performed to investigate the impact of CO_2 pressure on the differential pressure profile, relative permeability of CO_2, and residual water saturation. The drainage floodings have been conducted injecting pure gaseous CO_2, liquid and supercritical CO_2 phase into the deionised water saturated core sample. The results would provide important insights about the impact of CO_2 phase on its injectivity, water or oil production rate, CO_2-water displacement and CO_2 migration in a sandstone reservoir.

2 Materials and Experimental Setup

The unsteady state dynamic drainage experiments (CO_2-water displacements) were conducted on a prototypical sandstone core sample from Guillemot A Field in the North Sea. The core sample is 1 inch in diameter and 3 inches in length as shown in Fig. (2).

The average porosity and absolute water permeability of the core sample were about 14% and 15.8mD, respectively. Before the CO_2-water displacement, the pore volume, porosity and absolute water permeability were determined. The weight difference between the dry and the wet core sample was used to calculate the core sample pore volume and porosity. The absolute water permeability was calculated by using the average pressure difference and the water flowrate under quasi-steady state conditions. The water used in this study was deionized.

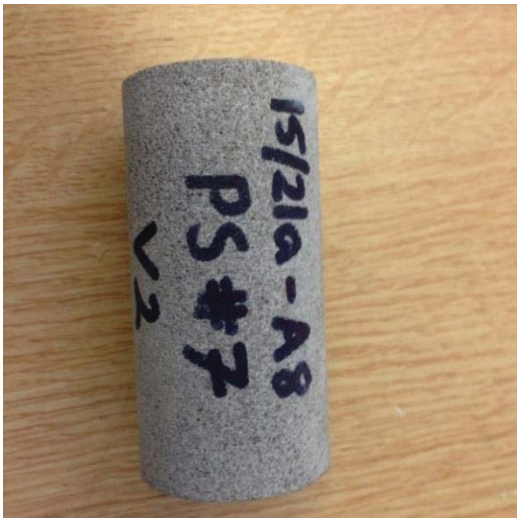

Fig. (2) Core sample used in this study

2.1 Experimental Setup

Fig. (3) Shows the core-flooding setup used to conduct the CO_2 (gas-liquid-supercritical)–water displacements. The experimental system consists of two high-pressure syringe pumps (Teledyne ISCO, Lincoln, NE, United States) with flowrate ranging from 0.0001 to 25 ml/min for CO_2 injection and CO_2 collection, a core holder, a water bath (GD 100) to control the temperature, a confining pressure pump (CM400) and a vacuum pump (Edwards, Model E2M5). A LabVIEW program was built to record the readings from the pressure transducers (UNIK 5000 pressure-sensor, 0-100bar) at the inlet and the outlet of the core sample.

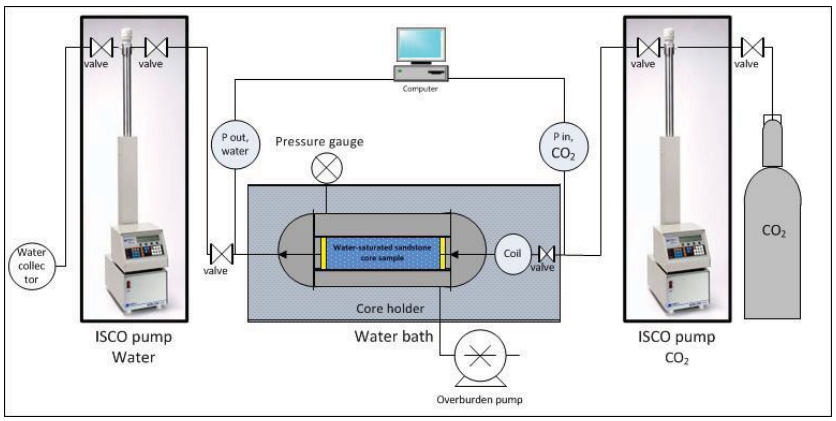

Fig. (3) The experimental setup for CO_2 (gas-liquid-supercritical)–water displacements.

3 CO_2- water displacement procedure

The unsteady state CO_2-WATER displacements, gasCO_2-WATER displacement, LiquidCO_2-WATER displacement and supercriticalCO_2-WATER displacement were conducted on a sandstone core sample.

The core sample was wrapped into a shrinkable Teflon tube followed by a rubber sleeve and then placed inside the core holder. The core holder was mounted horizontally inside the water bath. The confining pressure was maintained at about 135 bars, which is always higher than the pore pressure to prevent fluid bypassing.

Prior to each flooding experiment, a constant pressure was applied to the entire system using the syringe pump at each end. The water bath was set to the required temperature.

During the experiment, the fluid flowrate and pressure were controlled by two high pressure syringe pumps (Teledyne ISCO, Lincoln, NE, United States) placed under room conditions. The transient behavior of the inlet pressure, the outlet pressure and the outlet fluid (water and CO_2) flowrate were closely monitored and analyzed. The inlet and the outlet pressure transducer readings were recorded every six seconds using the LabVIEW software, in order to calculate the pressure difference between the inlet and the outlet. At the end of each experiment, the core sample weight was measured using a Sartorius weighing scale with a resolution of 0.0001g. The residual water saturation (Swr) with respect to the injected CO_2 was calculated as the ratio of the produced water to the total core pore volume.

It should be noticed that since the injecting and collecting pumps are placed under room temperature, the injected CO_2 experiences an expansion. The density of the injected CO_2 varies as the CO_2 enters the water bath. The density ratio (defined in Equation 1) suggested by Perrin and Benson [29] has been used to calculate the real injection rate inside the core sample. For instance, at experimental pressure of 40 bars, a flowrate of 1 cm^3/min at 20°C becomes 1.108cm^3/min at 33°C. However, at experimental pressure of 70 bars, it becomes 3.288cm^3/min.

$$\frac{d_{CO2}{}^{20^oC,40\ bar}}{d_{CO2}{}^{33^oC,40\ bar}} \qquad (1)$$

4 Results and discussions

To gain a deep insight into the CO_2-WATER dynamic drainage displacements and the effect of CO_2 phase, the inlet and outlet pressure, outlet CO_2 and water flow rates, the estimated residual water saturation and endpoint relative CO_2 permeability were measured and analyzed.

4.1 Effect of CO_2 phase on the differential pressure profile as experimental pressure increases.

Fig. (4) to Fig. (6) Show that the differential pressure profile is characterized by a high reduction, mainly during the first period (i.e before CO_2 breakthrough). This reduction occurs as the CO_2/water interface proceeds along the core sample, thereby a more viscous fluid (water) is being replaced by a less viscous fluid (CO_2) [30].

The results indicate that the differential pressure profile is a function of CO_2 phase, particularly during

the first period. During the first period, the differential pressure profile of liquid CO_2 characterized by a quasi-pressure reduction while that of gaseous and supercritical CO_2 phases characterized by a high reduction.

The results also show that the response of the differential pressure profile to the increase in the experimental pressure is a function of CO_2 phase, too. For sub critical CO_2 phases (gaseous and liquid CO_2), the increase in the experimental pressure led to an increase the differential pressure profile while for supercritical phase the increase in the pressure caused a reduction in the pressure differential pressure profile.

Fig. (4) shows that the increase in the experimental pressure led to an increase in the rate of the pressure difference (PD) oscillation, a rise in the maximum-pressure difference (P_{dmax}), a rise in the quasi-pressure difference, and a reduction in the time required to achieve the maximum pressure difference (corresponding time). The quasi pressure difference in this study refers to the pressure difference at the end of the core flooding. The rate of the change in the PD oscillations, pressure differences, and corresponding time depend on the magnitude of the experimental pressure. The highest change occurred as the experimental pressure increased from low (40 and 50 bars) to higher pressure displacements (70 bars).

For illustration, as the experimental pressure increased from 40 to 50 bars, the rate of PD oscillations increased by around 33% and the Pdmax by about 2.50 % while the quasi pressure difference was constant at around 1 bar. The corresponding time declined by approximately 17 %. However, as the pressure increased from 50 to 70 bars, the PD oscillations increased by 225%, the Pdmax by around 9%, and the quasi pressure difference by 165%. The corresponding time dropped considerably by around 78%. The high reduction in the corresponding time as the pressure increased from 50 to 70 bars can be related mainly to gas density and CO_2 injection rate. As pressure increases, the gaseous CO_2 became denser and the injection rate increased due to temperature difference, for more information see page 80. Hence, gaseous CO_2 needed much less time to be compressed to the required pressure. On the other hand, the high increase in the quasi pressure difference can be related mainly to the increase in the applied viscous forces due to increasing viscosity and the injection injection rate because of gas expansion.

The maximum pressure differences can be related to the pressure drop due to viscous forces and that due to interfacial tension forces. As the experimental pressure increases, the pressure drop due to viscous forces increases while that due to interfacial forces reduces. This is because the increase in pressure causes an increase in gas viscosity and CO_2 injection rate as well as a reduction in the CO_2-

water IFT tension and increase in the contact angle because of increasing CO_2 solubility [31, 32]. Hence, the observed increase in the maximum pressure difference with increasing pressure is because viscous forces became larger than interfacial forces.

It should be noticed that the observed fluctuations in the differential pressure profile (PD oscillations) are due to the ratio of the interfacial forces to viscous forces. The phenomenon of PD oscillations occurs when the interfacial forces becomes large enough to overcome viscous forces. The result is a complete blocking of water production until the pressure builds up to overcome the interfacial forces and open closed flow paths [30]. The complete blocking of production occurs due to the occurrence of the re-imbibition process. It has been observed by Plug and Bruining that an alternate drainage and imbibition process occurs during CO_2 injection when the measurements close to the critical point of CO_2. This has been attributed to small perturbations that change the density and viscosity of CO_2 and temporary CO_2-wet behaviour [3]. The phenomenon of PD oscillations has been investigated in depth in a different study.

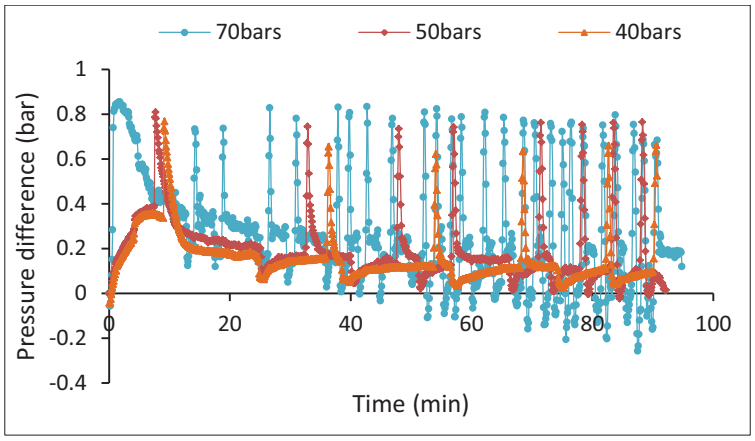

Fig. (4) Effect of pressure on the differential pressure profile of gas CO_2-water displacements conducted at 0.4 ml/min, 33 ^oC.

Fig. (5) shows that as the experimental pressure of liquid CO_2 increased, the maximum pressure difference increased by 17% (from 0.463 to 0.543 bar), and the quasi-pressure difference by around 5% (from 0.222 to 0.233 bars). The corresponding time was small and constant at around 0.5 min. Interestingly, the PD oscillations disappeared.

The disappearance of the oscillations and the small and constant corresponding time can be related to the dense nature of liquid CO_2 and the negligible impact of interfacial forces. The dense nature means that the pressure drop due to viscous forces is always higher than that due to interfacial forces, thereby no PD oscillations. Moreover, the dense nature of liquid CO_2 means much less corresponding time is required to reach the maximum pressure difference in comparison to gaseous CO_2. For instance, as the CO_2 phase changed from gaseous to liquid CO_2 state, the corresponding time decreased by around 71 % (from 1.7 to 0.5 min) as shown in Fig. (4) and Fig. (5).

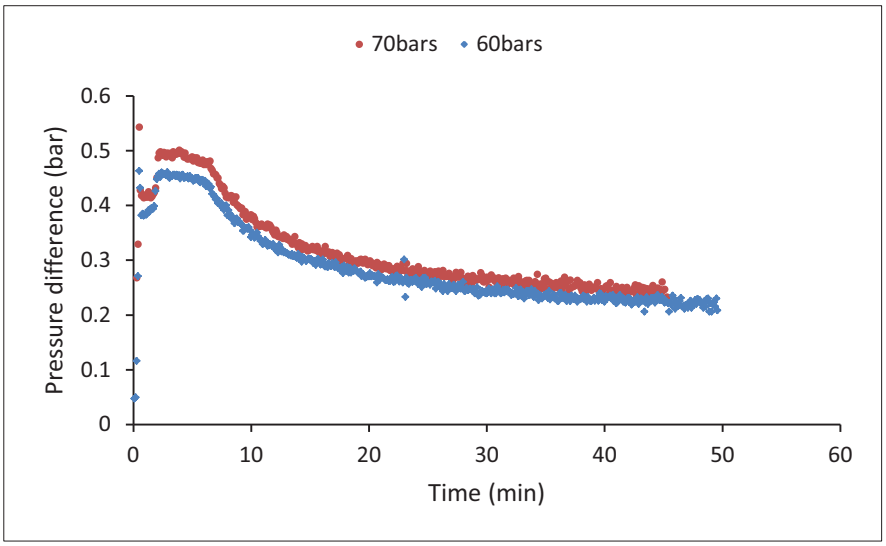

Fig. (5) Effect of pressure on the differential pressure profile of liquid CO_2-water displacements conducted at 0.4ml/min, and 20 ^{0}C.

On the other hand, Fig. (6) reveals that increasing pressure caused a significant reduction in the maximum and quasi pressure differences and the corresponding time of supercritical CO_2 phase. As the pressure raised from 75 to 90 bars, the maximum-pressure difference dropped by around 47 %, the quasi-pressure difference by around 39 %, and the corresponding time by around 68%.

The largest change in the maximum and the quasi-pressure differences occurred as the pressure increased from 80 to 90 bars. When the pressure increased from 75, 77, 80 to 90 bars, the maximum pressure difference decreased from around 1.121, 0.9275, 0.767, to 0.599 bars, and the quasi-pressure difference declined from 0.363, 0.3045, 0.281 to 0.221 bars. However, the corresponding times are 1.9, 0.8, 0.4, and 0.6 mins.

Fig. (6) suggest also that as the pressure increases, the differential pressure profile of supercriticalCO_2-water displacement transformed from the likeness of a gaseous CO_2 behaviour to a liquid CO_2 behaviour. For instance, the differential pressure profile of the 75 bars-experiment is very similar to that

of a typical high-pressure gasCO_2-water displacement while that of 90 bars is virtually identical to that of a typical liquid CO_2-water displacement. The similarity to a gaseous or liquid CO_2 behaviour has been decided based on the differential pressure profile, mainly during the first period. The differential pressure profile of the experiments conducted at gaseous CO_2 conditions characterizes by a sharp pressure reduction during the first period. On the other hand, the differential pressure profile of the experiments conducted at liquid CO_2 conditions characterizes by a quasi-stable pressure profile during the first period.

The reduction in the differential pressure profile can be related mainly to the reduction in the interfacial tension forces due to the drop in the CO_2-water interfacial tension and the increase in contact angle because of the increase in CO_2 solubility [32, 33].

The transformation of the differential pressure profile with increasing pressure proposes that the interfacial and viscous properties of supercritical CO_2 phase become similar to that of gaseous CO_2 phase at low pressures and similar to that of liquid CO_2 phase at high pressures. The liquid CO_2 characterized by a higher impact of viscous forces and a lesser impact of interfacial forces forces in comparison to gaseous CO_2. With increasing pressure, the impact of the viscous forces become higher while the impact of the interfacial forces become lesser. This because the increase in the experimental pressure leads to an increase in the CO_2 density and viscosity as well as a decrease in the interfacial tension and an increase in the contact angle due to increasing CO_2 solubility [3, 5]. For instance, as the pressure increased from 75 to 90 bars, the scCO_2 density increased from 410.255 to 666.69 kg/m^3, the CO_2 injection rate decreased from 0.798 to 0.506 ml/min, the viscosity increased from 33.3095 to 53.837 [10^{-6} (Pa s)], and the CO_2-water interfacial tension reduced from around 28 to 25 mN/m (34).

Moreover, it is expected also that as the pressure increases, the wettability of liquid and supercritical CO_2 phases might become very close at high pressure conditions. For supercritical CO_2, a potential wettability alteration towards hydrophobic wetting state might occur as pressure increases [32]. However, for liquid CO_2, the potential hydrophobic wetting state might occur due to phase transformation [8]. Yang et al. 2005 observed that as gaseous CO_2 phase transformed to liquid CO_2, the wetting state becomes hydrophobic [8].

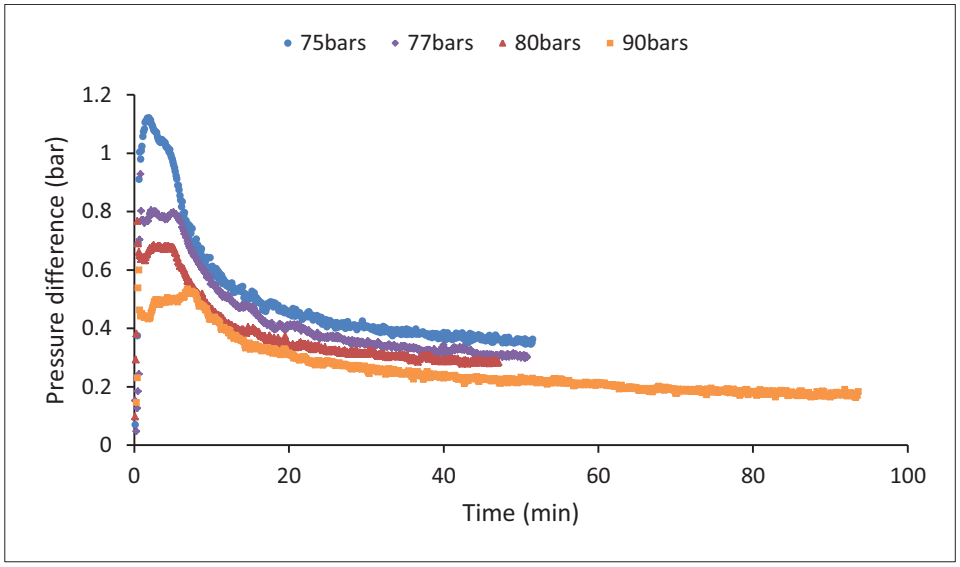

Fig. (6) Effect of pressure on the differential pressure profile of supercritical CO_2-water displacements conducted at 0.4ml/min, and 33 ^{0}C.

4.2 Effect of CO_2 phase on residual water saturation and relative permeability as experimental pressure increases

At the end of the core floodings, the volume of the produced water was measured, the system was depressurized to the atmospheric pressure to allow total degassing of the CO_2, and the core sample was weighed to obtain the residual water saturation. To calculate the relative CO_2 permeability using Darcy's law, the average differential pressure and the average CO_2 flow rate of the last period were used. The CO_2 viscosity at the experimental pressure and temperature was calculated using NIST CHEMISTRY Webbook website [35]. The relative permeability of the CO_2 is calculated at the residual water saturation. The determination of the relative permeability of CO_2 and its variation with the investigated parameters is of practical interest for CO_2 sequestration in subsurface formations [36].

Table (1) reveals that the relative permeability of the three CO_2 phases were in the range of 11-21% while the residual water saturations in the range of 36-42%. Both gaseous and supercritical CO_2 gave close relative permeabilities. Liquid CO_2 gave the highest relative permeabilities. The increase in the experimental pressure led to an increase in the relative permeability of CO_2 (K_{rCO2}) and a decline in the residual water saturation (S_{wr}). The scale of change depends on CO_2 phase. The increase in the K_{rCO2} can be attributed mainly to the increase in the CO_2 injection rate due to the high impact of gas expansion, for more information see page 80. The increase in injection rate might result in forcing the

CO_2 to flow through a wider range of pores of the core sample. The reduction in the S_{wr} can be attributed to the increase in the capillary number (Ca) and the reduction in mobility ratio (M).

For gaseous CO_2, increasing pressure from 40 to 70 bars at 33 ^oC caused the K_{rCO2} to increase by around 5.4 %, and the S_{wr} to decrease by around 4.7 %. The largest increase in K_{rCO2} and the highest reduction in the S_{wr} occurred as the pressure increased from low pressure displacements (40 and 50 bars) to high pressure displacements (70 bars). This can be attributed to a relatively high increase in the Ca and a high reduction in M.

For liquid CO_2, as the pressure increased from 40 to 70 bars at 20 ^oC, the K_{rCO2} increased very slightly by around 0.6 %, and the S_{wr} decreased by around 2.2 %. However, for supercritical CO_2, as the pressure increased from 75 to 90 bars at 33 ^oC, the K_{rCO2} increased significantly by around 8 %, and the S_{wr} decreased by around 1.5 %.

Table (1) Effect of pressure on the end-point relative permeability of CO_2, and residual water saturation.

Parameter	Experiment	Effective permeability (mD)	Relative permeability (%)	Residual water	Mobility ratio	Capillary number
Gaseous CO_2	40-0.4ml/min-33 ^oC	1.768	11.3	42.44	46.26	5.265E-08
	50-0.4ml/min-33 ^oC	1.987	12.7	40.89	44.56	6.250E-08
	70-0.4ml/min-33 ^oC	2.613	16.7	37.79	36.10	2.504E-07
Liquid CO_2	60-0.4ml/min-20 ^oC	3.188	20.3	36.9	14.3315	2.174E-07
	70-0.4ml/min-20 ^oC	3.248	20.7	36.3	13.3996	2.734E-07
Supercritical CO_2	75-0.4ml/min-33 ^oC	1.858	11.849	37.2	22.48	2.566E-07
	77-0.4ml/min-33 ^oC	2.207	14.077	37.4	19.53	2.594E-07
	80-0.4ml/min-33 ^oC	2.388	15.228	37.2	16.32	2.645E-07
	90-0.4ml/min-33 ^oC	3.128	19.949	35.7	13.91	2.965E-07

5 Conclusion

In this paper, the effect of CO_2 phase on the pressure and production profiles of CO_2-water drainage floodings has been investigated as the experimental pressure increases. The investigations were conducted for the three phases of CO_2 (gas, liquid, and supercritical). The results indicate a considerable influence of the CO_2 phase on the differential pressure profile, relative permeability of CO_2, and residual water saturation. The relative permeabilities of the three CO_2 phases were in the range of 11-21% while the residual water saturations were in the range of 36 to 42%. Both gaseous and supercritical CO_2 gave close relative permeabilities. Liquid CO_2 gave the highest relative permeabilities. The increase in the experimental pressure led to an increase in the relative permeability of CO_2 (K_{rCO2}) and a decline in the residual water saturation (S_{wr}). The scale of change depends on CO_2 phase.

The differential pressure profile is a function of CO_2 phase, particularly before CO_2 breakthrough. The differential pressure profile of liquid CO_2 characterized by a quasi-pressure reduction while that of gaseous and supercritical CO_2 phases characterized by a high reduction.

The response of the differential pressure profile to the increase in the experimental pressure is a function of CO_2 phase, too. For sub critical CO_2 phases (gaseous and liquid CO_2), the increase in pressure led to an increase the differential pressure profile while for supercritical phase the increase in the pressure led to a reduction in the pressure differential pressure profile.

For gaseous CO_2 phase, the increase in the experimental pressure led to an increase in the rate of the pressure difference (PD) oscillation, a rise in the maximum-pressure difference (P_{dmax}), an increase in the quasi-pressure difference, and a reduction in the time required to reach the Pdmax (the corresponding time). The highest change occurred as the pressure increased from low to high pressure (70 bars) displacements. As the experimental pressure increased from 40 to 50 bars, the rate of PD oscillations increased by around 33% and the Pdmax by about 2.50 % while the quasi pressure difference was constant at around 1 bar. The corresponding time declined by approximately 17 %. However, as the pressure increased from 50 to 70 bars, the PD oscillations increased by 225 %, the Pdmax by around 9 %, and the quasi pressure difference by 165 %. The corresponding time dropped considerably by around 78%.

For liquid CO_2 phase, increasing the experimental pressure from 60 to 70 bars caused the maximum pressure difference to increase by 17% and the quasi-pressure difference by around 5%. The corresponding time was constant at around 0.5 min. The differential pressure profile does not show pressure difference oscillations.

On the other hand, increasing pressure for supercritical CO_2 phase caused a significant reduction in the maximum and quasi pressure differences as well as the corresponding time. As the pressure raised from 75 to 90 for the experiments, the maximum-pressure difference dropped by around 47 %, the quasi pressure difference by around 39 %, and the corresponding time by around 68%. The largest change in the maximum and the quasi pressure differences occurred as the pressure increased from 80 to 90 bars.

The increase in the experimental pressure caused the differential pressure profile of scCO_2-water displacement to transform from the likeness of gas-displacement performance to that of liquid-displacement. For illustration, the differential pressure profile of the 75 bars-experiment is very similar to that of a typical high-pressure gasCO_2-water displacement while that of 90 bars-displacement becomes virtually identical to that of a typical LCO_2-water displacement.

References

1. Li Z, Dong M, Li S, Huang S. CO2 sequestration in depleted oil and gas reservoirs—caprock characterization and storage capacity. Energy Conversion and Management. 2006;47(11):1372-82.

2. Kaveh NS, Wolf K, Ashrafizadeh S, Rudolph E. Effect of coal petrology and pressure on wetting properties of wet coal for CO2 and flue gas storage. International Journal of Greenhouse Gas Control. 2012;11:S91-S101.

3. Plug W-J, Bruining J. Capillary pressure for the sand–CO2–water system under various pressure conditions. Application to CO2 sequestration. Advances in Water Resources. 2007;30(11):2339-53.

4. Tutolo BM, Luhmann AJ, Kong X-Z, Saar MO, Seyfried WE. CO2 sequestration in feldspar-rich sandstone: coupled evolution of fluid chemistry, mineral reaction rates, and hydrogeochemical properties. Geochimica et Cosmochimica Acta. 2015;160:132-54.

5. Espinoza DN, Santamarina JC. Water-CO2-mineral systems: Interfacial tension, contact angle, and diffusion—Implications to CO2 geological storage. Water resources research. 2010;46(7).

6. Bachu S. Sequestration of CO2 in geological media: criteria and approach for site selection in response to climate change. Energy conversion and management. 2000;41(9):953-70.

7. Shi J-Q, Xue Z, Durucan S. Supercritical CO2 core flooding and imbibition in Tako sandstone—Influence of sub-core scale heterogeneity. International Journal of Greenhouse Gas Control. 2011;5(1):75-87.

8. Yang D, Tontiwachwuthikul P, Gu Y. Interfacial interactions between reservoir brine and CO2 at high pressures and elevated temperatures. Energy & Fuels. 2005;19(1):216-23.

9. Liu N, Ghorpade SV, Harris L, Li L, Grigg RB, Lee RL, editors. The effect of pressure and temperature on brine-CO2 relative permeability and IFT at reservoir conditions. SPE Eastern Regional Meeting; 2010: Society of Petroleum Engineers.

10. Suekane T, Ishii T, Tsushima S, Hirai S. Migration of CO2 in Porous Media Filled with water. Journal of Thermal Science and Technology. 2006;1(1):1-11.

11. Riazi M, Sohrabi M, Bernstone C, Jamiolahmady M, Ireland S. Visualisation of mechanisms involved in CO2 injection and storage in hydrocarbon reservoirsand water-bearing aquifers. Chemical Engineering Research and Design. 2011;89(9):1827-40.

12. Saraji S, Piri M, Goual L. The effects of SO2 contamination, brine salinity, pressure, and temperature on dynamic contact angles and interfacial tension of supercritical CO2/brine/quartz systems. International Journal of Greenhouse Gas Control. 2014;28:147-55.

13. Herring AL, Andersson L, Newell D, Carey J, Wildenschild D. Pore-scale observations of supercritical CO2 drainage in Bentheimer sandstone by synchrotron x-ray imaging. International Journal of Greenhouse Gas Control. 2014;25:93-101.

14. Ott H, Pentland C, Oedai S. CO2–brine displacement in heterogeneous carbonates. International Journal of Greenhouse Gas Control. 2015;33:135-44.

15. Ott H, Berg S, Oedai S. Displacement and mass transfer of CO2/brine in sandstone. Energy Procedia. 2012;23:512-20.

16. Akbarabadi M, Piri M. Relative permeability hysteresis and capillary trapping characteristics of supercritical CO2/brine systems: An experimental study at reservoir conditions. Advances in Water Resources. 2013;52:190-206.

17. Pentland C, El-Maghraby R, Georgiadis A, Iglauer S, Blunt M. Immiscible displacements and capillary trapping in CO2 storage. Energy Procedia. 2011;4:4969-76.

18. Pentland CH, El-Maghraby R, Iglauer S, Blunt MJ. Measurements of the capillary trapping of super-critical carbon dioxide in Berea sandstone. Geophysical Research Letters. 2011;38(6).

19. Lopez O, Idowu N, Mock A, Rueslåtten H, Boassen T, Leary S, et al. Pore-scale modelling of CO2-brine flow properties at In Salah, Algeria. Energy Procedia. 2011;4:3762-9.

20. Alemu BL, Aker E, Soldal M, Johnsen Ø, Aagaard P. Influence of CO2 on rock physics properties in typical reservoir rock: a CO2 flooding experiment of brine saturated sandstone in a CT-scanner. Energy Procedia. 2011;4:4379-86.

21. Levine JS, Matter JM, Goldberg DS, Lackner KS, Supp MG, Ramakrishnan T. Two phase brine-CO2 flow experiments in synthetic and natural media. Energy Procedia. 2011;4:4347-53.

22. Bachu S. Drainage and imbibition CO2/brine relative permeability curves at in situ conditions for sandstone formations in western Canada. Energy Procedia. 2013;37:4428-36.

23. Qi R, Laforce T, Blunt M. Carbon Dioxide (CO2) Injection Design to Maximize Underground Reservoir Storage and Enhanced Oil Recovery (EOR). Developments and Innovation in Carbon Dioxide (CO2) Capture and Storage Technology (Ed MM Maroto-Valer), Woodhead Publishing Series in Energy, Oxford. 2010:169-84.

24. Pini R, Krevor SC, Benson SM. Capillary pressure and heterogeneity for the CO2/water system in sandstone rocks at reservoir conditions. Advances in Water Resources. 2012;38:48-59.

25. Saeedi A, Rezaee R, Evans B, Clennell B. Multiphase flow behaviour during CO2 geo-sequestration: Emphasis on the effect of cyclic CO2–brine flooding. Journal of Petroleum Science and Engineering. 2011;79(3):65-85.

26. Berg S, Ott H. Stability of CO2–brine immiscible displacement. International Journal of Greenhouse Gas Control. 2012;11:188-203.

27. Wollenweber J, Alles S, Busch A, Krooss B, Stanjek H, Littke R. Experimental investigation of the CO2 sealing efficiency of caprocks. International Journal of Greenhouse Gas Control. 2010;4(2):231-41.

28. Chang C, Zhou Q, Xia L, Li X, Yu Q. Dynamic displacement and non-equilibrium dissolution of supercritical CO2 in low-permeability sandstone: An experimental study. International Journal of Greenhouse Gas Control. 2013;14:1-14.

29. Perrin J-C, Benson S. An experimental study on the influence of sub-core scale heterogeneities on CO2 distribution in reservoir rocks. Transport in porous media. 2010;82(1):93-109.

30. Nutt C, editor The physical basis of the displacement of oil from porous media by other fluids: a capillary bundle model. Proceedings of the Royal Society of London A: Mathematical, Physical and Engineering Sciences; 1982: The Royal Society.

31. Bennion DB, Bachu S, editors. The impact of interfacial tension and pore size distribution/capillary pressure character on CO2 relative permeability at reservoir conditions in CO2-brine systems. SPE/DOE Symposium on Improved Oil Recovery; 2006: Society of Petroleum Engineers.

32. Yang D, Gu Y, Tontiwachwuthikul P. Wettability determination of the reservoir brine− reservoir rock system with dissolution of CO2 at high pressures and elevated temperatures. Energy & Fuels. 2007;22(1):504-9.

33. Plug W-J, Bruining J. Capillary pressure for the sand–CO 2–water system under various pressure conditions. Application to CO 2 sequestration. Advances in Water Resources. 2007;30(11):2339-53.

34. Bachu S, Bennion DB. Interfacial tension between CO2, freshwater, and brine in the range of pressure from (2 to 27) MPa, temperature from (20 to 125)° C, and water salinity from (0 to 334 000) mg· L− 1. Journal of Chemical & Engineering Data. 2008;54(3):765-75.

35. NIST Chemistry WebBook. Thermophysical Properties of Fluid Systems 2016 [cited 2016 01/12/2016].

36. Rathnaweera T, Ranjith P, Perera M. Effect of salinity on effective CO2 permeability in reservoir rock determined by pressure transient methods: An experimental study on Hawkesbury sandstone. Rock Mechanics and Rock Engineering. 2015;48(5):2093-110.